Hubbard model and Mott-Hubbard transition.

Pritish Karmakar *

May 20, 2025

Abstract

We review the Hubbard model and its extensions as a framework to describe electron correlation and the Mott metal-insulator transition. Starting from the atomic and band limits, we explore the emergence of Hubbard sub-bands and the Mott transition through Hubbard-I decoupling. The strong-coupling expansion leads to the t-J model, highlighting spin-exchange mechanisms. We then study the extended Hubbard model with emphasis on orbital physics and transition metal oxides. The role of super-exchange, charge-transfer effects are discussed in relation to real materials. Finally, the Dynamical Mean Field Theory (DMFT) approach is introduced to capture certain features of the HUbbard model, including emergence of sub-bands, the evolution of spectral weight.

Contents

1 Introduction

Metal, insulator and their characterization play an important role in condensed matter physics. We know in the absence of any potential, electrons behave as free particles and form a continuum of energy

*IISER Kolkata, Roll no: 21MS179, Mail: pk21ms179@iiserkol.ac.in.

states. However, in a crystalline solid, the presence of a periodic potential due to the lattice leads to the formation of energy bands. We charecterize metal and insulator in Band theory by the position of Fermi level. If the Fermi level lies within an energy band, the system behaves as a *metal*. In such a case, the density of states at the Fermi level is nonzero, i.e., $\rho(\epsilon_F) \neq 0$. Conversely, if the Fermi level lies within a band gap, the system is a *band insulator*, characterized by a vanishing density of states at the Fermi level: $\rho(\epsilon_F) = 0$.

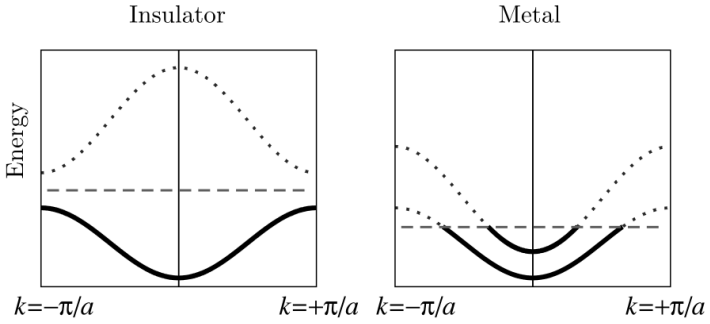

Figure 1: Schematic comparison of metallic and insulating band structures.

To quantify electron filling in a lattice, consider the electron density defined as

$$n = \frac{\text{Number of electrons}}{\text{Number of sites}} = \frac{N}{L}.$$

For a single non-degenerate band, $n = 1$ corresponds to a half-filled band, which typically results in metallic behaviour. On the other hand, $n = 2$ indicates a fully filled band, leading to an insulating state due to the absence of available states for conduction.

Interestingly, it has been experimentally observed in certain transition metal oxides that even at half-filling ($n = 1$), the system behaves as an insulator. This insulating state cannot be explained by conventional band theory and is referred to as a *Mott insulator*. The Mott insulating behavior arises from strong on-site Coulomb repulsion, which inhibits the hopping of electrons between lattice sites. As a result, the system becomes insulating despite having a partially filled band. This phenomenon shows the limitations of non-interacting band theory and its necessary to include the electron-electron interactions. A minimal theoretical model that captures the essential physics of Mott insulators is the *Hubbard model*, which incorporates both the kinetic energy of electrons (via hopping) and as well as the on-site Coulomb repulsion.

2 The Hubbard model

For our conventional non-interacting Band theory the Hamiltonian that describe the electron delocalization behaviour, is given by

$$H_t = \sum_{\langle ij \rangle \sigma} \left(t_{ij} c^\dagger_{i\sigma} c_{j\sigma} + \text{h.c.} \right) \tag{1}$$

where $c^\dagger_{i\sigma}$ and $c_{i\sigma}$ electron creation and annihilation operator in i-th lattice site. They follow typical fermionic anti-commutation relation. We want to incorporate the on-site Coulomb interaction term to describe Mott-like phenomena.

The Hubbard Hamiltonian captures both the electron delocalization and interaction, and consists of two components: a band (kinetic) term and an intra-site Coulomb term. It is given by

$$H = H_t + H_U = \underbrace{-\sum_{\langle ij\rangle\sigma}\left(t_{ij}c^\dagger_{i\sigma}c_{j\sigma} + \text{h.c.}\right)}_{\text{Band term}} + \underbrace{U\sum_j n_{j\uparrow}n_{j\downarrow}}_{\text{Coulomb term}}, \tag{2}$$

where $n_{j\uparrow} = c^\dagger_{j\uparrow}c_{j\uparrow}$.

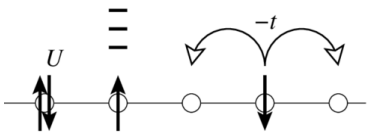

Figure 2: Schematic representation of the Hubbard model.

It is important to discuss certain symmetries of the Hubbard Hamiltonian. First is *spin-rotation invariance*. For that the only term we have to worry is the Coulomb term since it only interact with two different spins. One can convert it in spin operators using

$$n_{j\uparrow}n_{j\downarrow} = n_{j\uparrow} - S^+_j S^-_j = n_{j\downarrow} - S^-_j S^+_j,$$
$$n_{j\uparrow} - n_{j\downarrow} = 2S^z_j, \quad n^2_{j\sigma} = n_{j\sigma},$$

which leads to a spin-rotation invariance from :

$$H_U = \frac{1}{2}UN - \frac{2}{3}\sum_j S^2_j \tag{3}$$

Second one is electron-hole symmetry. As we will see later, it will reflect in phase diagram. We see that the following transformation from electron field operator to hole field operator:

$$c^\dagger_{j\sigma} \to c_{j\sigma}, \quad c_{j\sigma} \to c^\dagger_{j\sigma}$$
$$n_{j\sigma} \to 1 - n_{j\sigma}$$

does not change the form of the Hubbard Hamiltonian.

Exact diagonalization of the Hubbard Hamiltonian is nearly impossible. But two important limiting cases of the Hubbard model help in understanding its physical behaviour:

1. Band limit ($U/t = 0$): In this case, the interaction term becomes negligible. The system is effectively non-interacting and can be diagonalized in momentum space:

$$H = H_t = \sum_{k\sigma}\varepsilon_k c^\dagger_{k\sigma}c_{k\sigma}, \quad \varepsilon_k = -2t\sum_{i=1}^{d}\cos(k_i a),$$

where d is the spatial dimension and a is the lattice constant.

2. Atomic limit ($U/t \to \infty$): Here, the kinetic energy is suppressed and the electrons are localized due to strong repulsion. The Hamiltonian becomes diagonal in position space:

$$H = H_U = U\sum_j |d\rangle\langle d|_j, \quad |d\rangle_j = c^\dagger_{j\uparrow}c^\dagger_{j\downarrow}|0\rangle_j,$$

where $|d\rangle_j$ represents a doubly occupied site at position j. Between these two limits, the full Hubbard model cannot be solved exactly in general and remains a central challenge in strongly correlated electron systems. In the later section we will extensively discuss the limit where U/t is very small, that helps to describe the Mott transition and Mott insulator.

2.1 Hubbard sub-bands

Although the full Hubbard model cannot be solved exactly in general, certain intuitive features can still be extracted in specific limits. One such concept is the emergence of Hubbard subbands, particularly relevant in the strongly interacting system. In the Mott insulating case, where $U \gg t$, the kinetic term H_t can be treated as a perturbation over the interaction term H_U. This provides a basis for understanding the system in terms of atomic states slightly broadened by hopping.

To build intuition of the Hubbard sub-bands, consider the energy cost of different site occupancies in the atomic limit: say a singly occupied site corresponds to a state with energy $E_{\text{at}} = 0$. A doubly occupied site cost an additional Coulomb energy i.e., $E_{\text{at}} + U = U$. So we have two bands at energy 0 and U. When hopping is introduced perturbatively, these atomic levels broaden into bands. The approximate width of these bands is given by $W \sim 2zt$, where z is coordination number. Consequently, two subbands form: a lower Hubbard band centered around $E = 0$ and an upper Hubbard band centered around $E = U$.

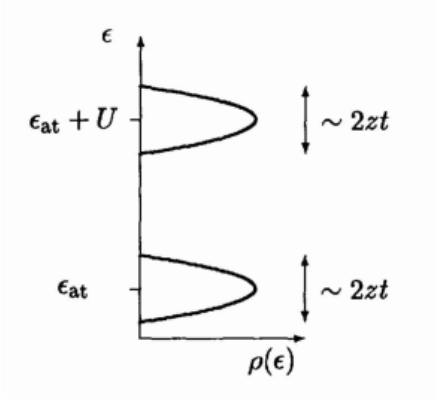

(a) Two subbands around $\epsilon = 0, U$ with bandwidth $W \sim 2zt$

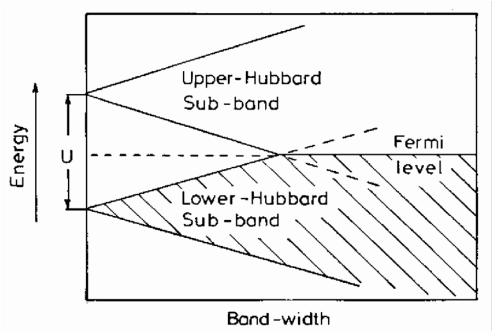

(b) Overlapping of two bands with increase of W.

Figure 3: Schematic illustration of Hubbard subbands in the strongly interacting limit.

It is significant to point out that its a occupation-number dependent band structure, not the usual band structure we see in band theory. If L be the number of sites, then the total number of available states is $2L$. In Hubbard sub-bands, each band has L states.

2.2 The Hubbard-I decoupling

The emergence of Hubbard sub-bands in the Mott regime can be analytically captured using the Hubbard-I decoupling scheme. Starting from the Hubbard model, we consider the equations of motion for the fermionic annihilation operator $c_{i\sigma}$, given by:

$$\omega c_{i\sigma} = [c_{i\sigma}, H] = \sum_j t_{ij} c_{j\sigma} + U n_{i,-\sigma} c_{i\sigma}. \tag{4}$$

Decoupling at this stage i.e., $n_{i,-\sigma} c_{i\sigma} \to \langle n_{i,-\sigma} \rangle c_{i\sigma}$, and doing Fourier transform will give

$$\omega = \varepsilon_k + \frac{1}{2} U \langle n \rangle ,$$

which is essentially the same result as obtained from band theory. This once again indicates metallic behaviour. Thus proceeding one step further:

$$\begin{aligned}\omega n_{i,-\sigma}c_{i\sigma} &= [n_{i,-\sigma}c_{i\sigma}, H] \\ &= \sum_j t_{ij} n_{i,-\sigma}c_{j,\sigma} + U n_{i,-\sigma}c_{i,\sigma} + \sum_j t_{ij}\left\{c^\dagger_{i,-\sigma}c_{j,-\sigma}c_{i,\sigma} - c^\dagger_{j,-\sigma}c_{i,-\sigma}c_{i,\sigma}\right\} \end{aligned} \tag{5}$$

and taking a mean-field decoupling and Hubbard 1 approximation we arrive at

$$\omega n_{i,-\sigma}c_{i\sigma} \approx \sum_j t_{ij}\left\langle n_{i,-\sigma}\right\rangle c_{j\sigma} + U n_{i,-\sigma}c_{i\sigma}. \tag{6}$$

Eliminating the composite operator $n_{i,-\sigma}c_{i\sigma}$ from eq. (4) and (6) and transforming to momentum space, one obtains the energy spectrum as:

$$\omega_\pm(k) = \frac{U + t(k)}{2} \pm \frac{1}{2}\sqrt{(U - t(k))^2 + 4Ut(k)\left\langle n_{i,-\sigma}\right\rangle}, \tag{7}$$

where $t(k) \equiv \varepsilon_k$ is the single-particle dispersion. At half-filling, $\langle n_{i,-\sigma}\rangle = 1/2$, and the expression simplifies to:

$$\omega_\pm(k) = \frac{1}{2}(U + \varepsilon_k) \pm \frac{1}{2}\sqrt{U^2 + \varepsilon_k^2}. \tag{8}$$

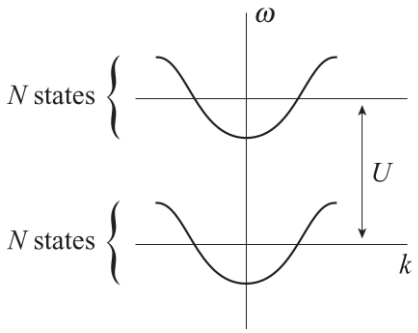

Figure 4: Hubbard sub-bands at half-filling. The plot shows the dispersion of the two Hubbard sub-bands $\omega_+(k)$ and $\omega_-(k)$ as a function of the wavevector k.

These two branches represent the lower and upper Hubbard bands, which are split by an energy gap of order U at large interaction strength. The formation of these sub-bands signals the breakdown of metallic behaviour at half filling.

3 Mott-Hubbard Transition

We now consider the system at half-filling, i.e., with electron density $n = 1$. In the Mott insulating regime ($U \gg t$), electrons primarily occupy the lower Hubbard sub-band, and double occupancy is energetically restricted. To describe the local excitation, it is useful to define a local basis at each site j

(and corresponding energy in atomic limit):

$$
\begin{aligned}
&|0\rangle_j : \text{empty site}, \quad H_U = 0 \\
&|\uparrow\rangle_j = c^\dagger_{j\uparrow} |0\rangle_j , \quad H_U = 0 \\
&|\downarrow\rangle_j = c^\dagger_{j\downarrow} |0\rangle_j , \quad H_U = 0 \\
&|d\rangle_j = c^\dagger_{j\uparrow} c^\dagger_{j\downarrow} |0\rangle_j , \quad H_U = U
\end{aligned}
$$

Note that due to fermionic anti-commutation relation $|d\rangle_j = c^\dagger_{j\uparrow} c^\dagger_{j\downarrow} |0\rangle_j \neq c^\dagger_{j\downarrow} c^\dagger_{j\uparrow} |0\rangle_j$. Although single occupancy costs no energy, virtual hopping processes still require access to doubly occupied states. For example, the hopping process

$$|\uparrow\rangle_i |\downarrow\rangle_j \to |0\rangle_i |d\rangle_j \to |\downarrow\rangle_i |\uparrow\rangle_j$$

involves a virtual transition to a doubly occupied state $|d\rangle_j$ in the upper Hubbard band. Therefore, knowing the band gap ($\sim U$) and bandwidth ($\sim 2zt$) is extremely important. As the ratio U/t is decreased, the separation between the Hubbard sub-bands diminishes due to increasing band broadening. This evolution is shown schematically in Fig. 5.

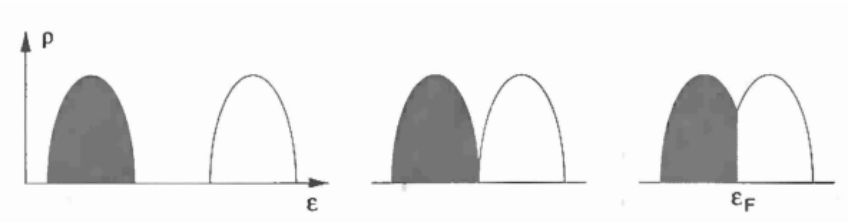

Figure 5: Evolution of the Hubbard bands with decreasing U/t. The Fermi level is right in between them for the half-filling case.

At a critical value of U/t (shown in the middle figure in 5), typically around $(U/t)_{\text{cr}} \sim 2z$, the lower and upper Hubbard bands begin to overlap. This marks the Mott-Hubbard transition from an insulating to a metallic state as virtual hopping process takes place by compensating the Coulomb term with kinetic term. The density of states at the Fermi level, $\rho(\epsilon_F)$, increases continuously from zero in the insulating phase to a finite value in the metallic phase. This transition seems second-order in nature. However, when long-range Coulomb interactions are taken into account, the transition can become first-order, showing a discontinuous jump in $\rho(\epsilon_F)$.

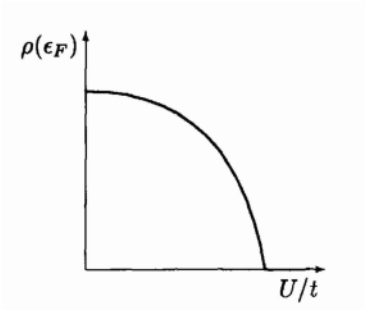

Figure 6: Second order change of density of state in Fermi level with U/t.

3.1 Phase diagram: U/t vs n

The qualitative features of the Mott-Hubbard transition can be shown in the $(U/t,\, n)$ parameter space, as shown in Fig. 7. The diagram exhibits symmetry about half-filling ($n = 1$), which arises from electron-hole symmetry inherent in the Hubbard model, as discussed before. At exact half-filling i.e., $n = 1$, the system undergoes a Mott-Hubbard metal-insulator transition as U/t crosses a critical threshold $(U/t)_{\text{cr}}$. Above this critical value, the system is in a Mott insulating state. Interestingly, the Mott insulator also exhibits long-range *antiferromagnetic* order due to super-exchange interactions mediated by virtual hopping. This order disappears away from half-filling as hopping is not restricted by H_U, where the system behaves as a *paramagnetic metal*.

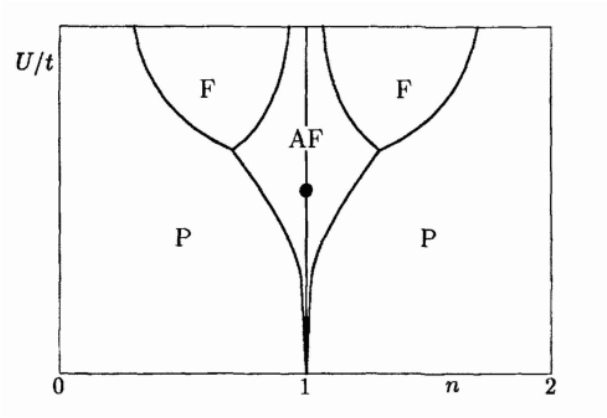

Figure 7: Schematic mean-field phase diagram of cubic lattice in the U/t vs. n plane. Black dot shows the point of Mott-Hubbard transition.

One may worry that to achieve exact $n = 1$ is nearly impossible. But near half-filling, the system exhibits remarkable robustness. Even with slight doping (still $n \approx 1$), the small number of added carriers, density of order $\sim |n - 1|$, can become localized due to disorder, leading to non-conducting behavior. This phenomenon is related to *Anderson localization*.

Qualitatively it can be understood why such antiferromagnetic order gives insulating state. Consider the ground state antiferromagnetic (Neel) ordered state as shown in the figure 8. In low energy excitation, we have an extra $|\downarrow\rangle$ current carrying electron trying to hop through the Neel ordered state. But it can not hop in either side because of the Pauli's excursion principle. Thus strongly antiferromagnetic order protect the insulating behaviour of the system.

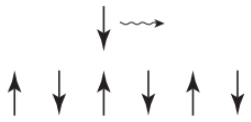

Figure 8: Current carrying electron hopping through a Neel ordered state.

4 Solving the Hubbard Model: Large U/t Limit

In the large U/t limit of the Hubbard Hamiltonian $H = H_U + H_t$, the H_t acts as perturbation over H_U. In zeroth order of t, we have atomic limit and corresponding two band separated by energy U. But the hopping term in the Hubbard Hamiltonian mixes states from different sub-bands, namely, the

lower and upper Hubbard bands by virtual hopping of electrons. To analyse the low-energy excitation while preventing such mixing, we perform a canonical transformation that decouples these bands up to a desired order in t/U. Canonical transformation is nothing but a unitary rotation over the Hilbert space of the problem such that we achieve our goal. The idea of canonical transformation here is as follows: We do a canonical transformation such that the basis state does not mix in upto order $\sim t$ which gives the $t-J$ model, further correction can be made step by step upto order $\sim t^2$ then $\sim t^3$ etc.

We begin by introducing projection operators for the local Hilbert space at site j:

$$\begin{aligned}
P_{j0} &= |0\rangle_j \langle 0|_j = (1-n_{j\uparrow})(1-n_{j\downarrow}) \\
P_{j\uparrow} &= |\uparrow\rangle_j \langle \uparrow|_j = n_{j\uparrow}(1-n_{j\downarrow}) \\
P_{j\downarrow} &= |\downarrow\rangle_j \langle \downarrow|_j = n_{j\downarrow}(1-n_{j\uparrow}) \\
P_{jd} &= |d\rangle_j \langle d|_j = n_{j\uparrow}n_{j\downarrow}
\end{aligned}$$

By using the projection operator we categorize all possible local excitation dictated by H_t in three categories: one where total number of doubly occupied state increases, one where it decreases and one where it remain same.

The hopping term H_t is then partitioned into three components:

$$H_t = H_t^+ + H_t^- + H_t^0 \tag{9}$$

where:

- H_t^+: increases the number of doubly occupied states (e.g., $|\uparrow\rangle_i |\downarrow\rangle_j \to |0\rangle_i |d\rangle_j$),
- H_t^-: decreases the number of doubly occupied states (e.g., $|0\rangle_i |d\rangle_j \to |\uparrow\rangle_i |\downarrow\rangle_j$),
- H_t^0: preserves the number of doubly occupied states (e.g., $|\uparrow\rangle_i |0\rangle_j \to |0\rangle_i |\uparrow\rangle_j$, or $|\uparrow\rangle_i |d\rangle_j \to |d\rangle_i |\uparrow\rangle_j$).

The exact form of these Hamiltonian is given below:

$$\begin{aligned}
\mathcal{H}_t^+ &= -t \sum_{\langle i,j\rangle} \sum_{\sigma} \left[\hat{n}_{i-\sigma} c_{i\sigma}^\dagger c_{j\sigma} (1-\hat{n}_{j-\sigma}) + \hat{n}_{j-\sigma} c_{j\sigma}^\dagger c_{i\sigma} (1-\hat{n}_{i-\sigma}) \right] \\
H_t^- &= -t \sum_{\langle i,j\rangle} \sum_{\sigma} \left[(1-\hat{n}_{i-\sigma}) c_{i\sigma}^\dagger c_{j\sigma} \hat{n}_{j\sigma} + (1-\hat{n}_{j-\sigma}) c_{j\sigma}^\dagger c_{i\sigma} \hat{n}_{i\sigma} \right] \\
H_t^0 &= -t \sum_{\langle i,j\rangle} \sum_{\sigma} \left[(1-\hat{n}_{i-\sigma}) c_{i\sigma}^\dagger c_{j\sigma} (1-\hat{n}_{j-\sigma}) + \hat{n}_{i-\sigma} c_{i\sigma}^\dagger c_{j\sigma} \hat{n}_{j-\sigma} + h.c. \right]
\end{aligned}$$

The goal is to perform a canonical (unitary) transformation to get an effective Hamiltonian, of the form:

$$H_{\text{eff}} = e^{iS} H e^{-iS} \tag{10}$$

with the generator $S = -\frac{i}{U}(H_t^+ - H_t^-)$, carefully chosen to eliminate mixing between the Hubbard sub-bands to leading order in t. Expanding to second order using the BCH formula, we obtain:

$$\begin{aligned}
H_{\text{eff}} &= H + i[S,H] + \frac{i^2}{2}[S,[S,H]] + \cdots \\
&\approx H_t^0 + H_U + \frac{1}{U}[H_t^+, H_t^-] + \cdot
\end{aligned}$$

There are no terms upto order $\sim t$ in the which increase or decrease the number of doubly occupied state occurs, so the desires goal to decouple the bands is achieved.

The commutator $[H_t^+, H_t^-]$ generates an effective spin interaction. One can identify that as:

$$[H_t^+, H_t^-] \longrightarrow \frac{2t^2}{U}\left(\vec{S}_i \cdot \vec{S}_j - \frac{1}{4}n_i n_j\right) + \text{Three-sites term}(\sim \frac{t^2}{U}) \tag{11}$$

Neglecting the Three-sites term, this yields the effective low-energy model known as the t-J model:

$$\begin{aligned} H_{\text{eff}} = &- t\sum_{\langle ij\rangle\sigma}(1-n_{i,-\sigma})\, c_{i\sigma}^\dagger c_{j\sigma}\,(1-n_{j,-\sigma}) \\ &+ J\sum_{\langle ij\rangle}\left(\vec{S}_i\cdot\vec{S}_j - \frac{1}{4}n_i n_j\right), \quad \text{where } J = \frac{4t^2}{U} \end{aligned} \tag{12}$$

Further one should aware of the 3-sites term of the Hamiltonian as it comes with order $\sim \frac{t^2}{U}$. The excitations are as shown in fig. 9. The cost we have to pay to eliminate $H_t^+ + H_t^-$ term by the canonical transformation is generating new mixing terms by 3-sites hopping shown in fig. 9b.

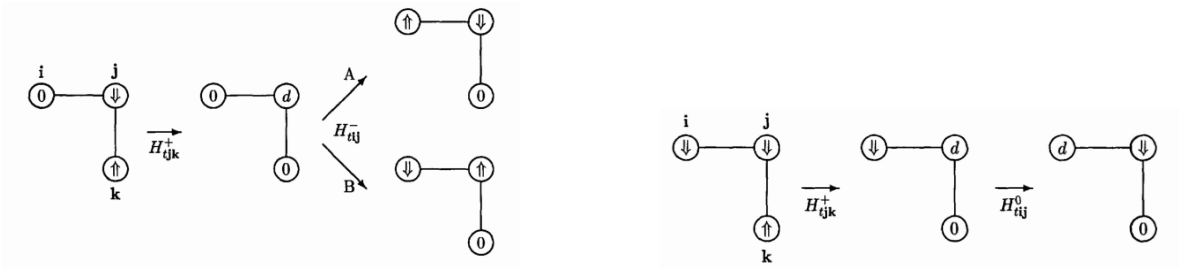

Figure 9: Two figure shows 3-sites hopping process in the effective hamiltonian.

The t-J model effectively captures the interplay of charge motion and spin correlations in the large-U regime of the Hubbard model. It becomes particularly relevant for studying doped Mott insulators and strongly correlated electron systems.

5 The t-J model

The t–J model derived via a canonical transformation from the Hubbard model captures the low-energy physics in the large-U regime by excluding virtual states involving doubly occupied sites up order $\sim t$. In this approximation, higher-order exchange processes — such as three-site or ring exchanges — are neglected. These processes would involve intermediate states like $|d\rangle$ (doubly occupied sites), which are absent in the second-order effective theory.

To account for these contributions, one can consider a more refined canonical transformation including higher-order terms. For instance, the generator may be expanded as $S = -\frac{i}{U}(H_t^+ - H_t^-) + S^{(2)}$, where $S^{(2)}$ is constructed to eliminate mixing of states involving double occupancy at higher orders.

At half-filling ($n_{i\sigma} = 1$), the charge degrees of freedom are frozen due to the strong on-site repulsion, and the effective low-energy Hamiltonian reduces to a pure antiferromagnetic model:

$$H_{\text{eff}} = J\sum_{\langle ij\rangle}\vec{S}_i\cdot\vec{S}_j,$$

which describes an *antiferromagnetic Heisenberg model* with exchange interaction $J = 4t^2/U$.

This kinetic exchange mechanism energetically favours antiferromagnetic alignment of neighbouring spins with energy gain associated with such superexchange interactions scales as $-t^2/U$ and results in a singlet ground state. Also on can argue that, for ferromagnetic ground state there is no virtual hopping (of the form $|\uparrow\rangle_i |\downarrow\rangle_j \to |0\rangle_i |d\rangle_j \to |\downarrow\rangle_i |\uparrow\rangle_j$) with the neighbourhood due to Pauli's excursion principle. But for antiferromagnetic ground state virtual hopping is possible, associate to which the second order perturbative energy gain is $\sim -t^2/U$ where U is the energy difference between singly occupied state and intermediate doubly occupied state. It highlighting the emergence of magnetic order in Mott insulators even in the absence of explicit spin-spin interactions in the original Hubbard model.

6 Many-Body Approach: Extended Hubbard Model

Here we use many-body approach to arrive at the Hubbard model and an extension of it. Till now we do not explicitly include the long-range Coulomb interactions in our system. Incorporating the effects of long-range Coulomb interactions and beyond nearest-neighbour hopping leads us to the extended Hubbard model, where the total Hamiltonian can be expressed as $H = H_{\text{tb}} + H_{\text{coulomb}}$, with the tight-binding part H_{tb} describing single-particle hopping and H_{coulomb} representing electron-electron interactions.

In tight-binding model the electronic states are expanded in terms of localized Wannier functions $\Phi_{g_i,\sigma}(r)$, centered at lattice sites g_i, which are constructed as a superposition of Bloch functions:

$$\Phi_\sigma(r - g_i) \equiv \Phi_{g_i,\sigma}(r) = \frac{1}{\sqrt{L}} \sum_k e^{-ikg_i} \phi_{k,\sigma}(r). \tag{13}$$

For single-band system this Wannier function approximately same as the localized orbital wave function. The field operator can then be expressed in either momentum or real space as

$$\psi^\dagger_\sigma(r) = \sum_k \phi^*_{k,\sigma}(r) c^\dagger_{k,\sigma} = \sum_{g_i} \Phi^*_{g_i}(r) c^\dagger_{i,\sigma}, \tag{14}$$

where the operators $c_{i,\sigma}$ and $c^\dagger_{i,\sigma}$ obey standard fermionic anti-commutation relations.

The one-body (tight-binding) Hamiltonian takes the form

$$H_{(1)} = \sum_\sigma \int dr\, \psi^\dagger_\sigma(r) H_{\text{tb}} \psi_\sigma(r) = -\sum_{i \neq j,\sigma} t_{ij} c^\dagger_{i\sigma} c_{j\sigma} + \epsilon \sum_{j\sigma} n_{j\sigma}, \tag{15}$$

where t_{ij} denotes the hopping amplitude between sites i and j, and ϵ is the on-site energy.

The interaction part of the Hamiltonian, $H_{(2)}$, originates from the two-body Coulomb repulsion:

$$\begin{aligned} H_{(2)} &= \sum_{\sigma_1,\sigma_2} \iint dr_1\, dr_2, \psi^\dagger_{\sigma_1}(r_1) \psi^\dagger_{\sigma_2}(r_2) H_{\text{coulomb}} \psi_{\sigma_2}(r_2) \psi_{\sigma_1}(r_1) \\ &= \sum_{ijkl} \sum_{\sigma_1,\sigma_2} V(g_i, g_j, g_k, g_l)\, c^\dagger_{i\sigma_1} c^\dagger_{j\sigma_2} c_{l\sigma_2} c_{k\sigma_1}, \end{aligned} \tag{16}$$

where

$$V(g_1, g_2, g_3, g_4) = \int dr_1 \int dr_2\, \Phi^*(r_1 - g_1) \Phi^*(r_2 - g_2) \frac{e^2}{|r_1 - r_2|} \Phi(r_1 - g_3) \Phi(r_2 - g_4).$$

This two-body Hamiltonian can be decomposed into several contributions:

- H_U: Intra-site Coulomb repulsion, corresponding to the standard Hubbard term,
- H_V: Inter-site Coulomb repulsion between electrons at different sites,
- H_F: Direct exchange interactions,
- H_X: Density-dependent hopping processes,
- H_Y: Simultaneous (correlated) hopping processes.

The exact expressions of these terms are as follows:

$$H_U = U \sum_j n_{j\uparrow} n_{j\downarrow}, \tag{17a}$$

$$H_V = V \sum_{\langle i,j \rangle} \sum_{\sigma_1,\sigma_2} \hat{n}_{i\sigma_1} \hat{n}_{j\sigma_2}, \tag{17b}$$

$$H_F = F \sum_{\langle i,j \rangle} \sum_{\sigma_1,\sigma_2} c^\dagger_{i\sigma_1} c^\dagger_{j\sigma_2} c_{i\sigma_2} c_{j\sigma_1} = -2F \sum_{\langle i,j \rangle} \left(\vec{S}_i \cdot \vec{S}_j + \frac{1}{4} \hat{n}_i \hat{n}_j \right) \tag{17c}$$

$$H_X = X \sum_{\langle i,j \rangle} \sum_{\sigma} \left(c^\dagger_{i\sigma} c_{j\sigma} + h.c. \right) \left(\hat{n}_{i-\sigma} + \hat{n}_{j-\sigma} \right) \tag{17d}$$

$$H_Y = Y \sum_{\langle i,j \rangle} \left(c^\dagger_{i\uparrow} c^\dagger_{i\downarrow} c_{j\downarrow} c_{j\uparrow} + h.c. \right) \tag{17e}$$

Thus our final form of Hamiltonian is $H = H_{\text{Hubbard}} + H_V + H_F + H_X + H_Y$. These additional features enrich the physics of the model significantly allows several other meaningful contributions.

7 Hubbard Model: Orbital Ordering and Orbital Degeneracy

We now extend the Hubbard model to include two orbitals per site, labeled a and b, with orbital wave-functions $\Phi^a_{i\sigma}$ and $\Phi^b_{i\sigma}$, and corresponding fermionic operators $c^\dagger_{ia\sigma}$ and $c^\dagger_{ib\sigma}$. We assume that there is no mixing between orbitals during hopping.

To capture the relevant physics, we consider a simplified two-site, two-orbital Hubbard Hamiltonian composed of three parts - hopping part, interacting part and spin-flipping part as follows:

$$H_{\text{hop}} = -\sum_{\sigma} \left[t_a \left(c^\dagger_{1a\sigma} c_{2a\sigma} + \text{h.c.} \right) + t_b \left(c^\dagger_{1b\sigma} c_{2b\sigma} + \text{h.c.} \right) \right], \tag{18a}$$

$$H_{\text{int}} = \sum_{j=1}^{2} \left[U_a n_{ja\uparrow} n_{ja\downarrow} + U_b n_{jb\uparrow} n_{jb\downarrow} + U_{ab} \sum_{\sigma_1,\sigma_2} n_{ja\sigma_1} n_{jb\sigma_2} - 2J \left(S^z_{ja} S^z_{jb} - \frac{1}{4} \right) \right], \tag{18b}$$

$$H_{\text{flip}} = -J \sum_{j=1}^{2} \left(c^\dagger_{ja\uparrow} c_{ja\downarrow} c^\dagger_{jb\downarrow} c_{jb\uparrow} + c^\dagger_{ja\downarrow} c_{ja\uparrow} c^\dagger_{jb\uparrow} c_{jb\downarrow} \right), \tag{18c}$$

where $S^z_{ja} = \frac{1}{2}(n_{ja\uparrow} - n_{ja\downarrow})$. The total Hamiltonian is given by $H = H_{\text{hop}} + H_{\text{int}} + H_{\text{flip}}$. A key physical insight is that the direct exchange interaction between two orthogonal orbitals on the same atom tends to favour a spin-*triplet* configuration as the lowest energy state, in accordance with Hund's rule. This leads to the coefficient $-2J$ of the forth term in H_{int}. The coefficient $-J$ in H_{flip} comes from spin rotation invariance of the system.

At half-filling ($n = 1$), different hopping channels lead to different ground state preferences depending on the orbitals involved. For intra-orbital hopping in the a-orbital channel, the Hamiltonian is given by

$$H_a = -\sum_{\sigma} t_a \left(c^{\dagger}_{1a\sigma} c_{2a\sigma} + \text{h.c.} \right) + \sum_{j=1}^{2} U_a n_{ja\uparrow} n_{ja\downarrow}, \tag{19}$$

so virtual hopping processes lead to a spin-singlet ground state, with an energy gain of approximately

$$E_{a,\text{singlet}} \sim -\frac{4t_a^2}{U_a}.$$

A similar mechanism operates for the b-orbital channel, yielding

$$E_{b,\text{singlet}} \sim -\frac{4t_b^2}{U_b}.$$

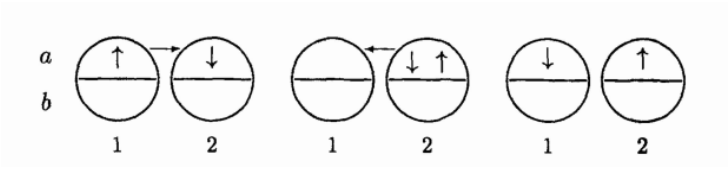

Figure 10: Intra-orbital (a-a) hopping favouring singlet state.

However, when electrons occupy different orbitals on neighbouring sites (e.g., a and b), and assuming $U_{ab} < U_a, U_b$, the exchange favours a spin-triplet ground state. The Hamiltonian is given by

$$H_{ab} = H_{\text{hop}} + \sum_{j=1}^{2} \left[U_{ab} \sum_{\sigma_1, \sigma_2} n_{ja\sigma_1} n_{jb\sigma_2} - 2J \left(S^z_{ja} S^z_{jb} - \frac{1}{4} \right) \right] \tag{20}$$

The corresponding energy scale is given by

$$E_{ab,\text{triplet}} \sim -\frac{(t_a + t_b)^2}{U_{ab} - J}.$$

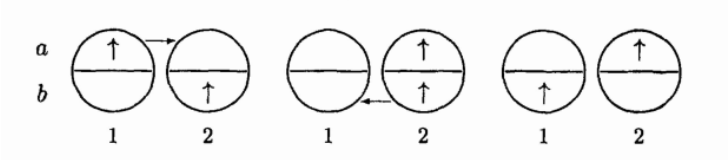

Figure 11: Inter-orbital (a-b) hopping favouring triplet state.

This behaviour reveals a correlation between spin and orbital degrees of freedom. The system tends to develop *spin ferromagnetism* coexisting with *orbital anti-ferromagnetism*. Specifically, when neighbouring sites occupy the same orbital, the ground state favours spin singlets; whereas when different orbitals are involved, the system favours spin triplets. This type of coupled spin-orbital ordering is a central feature in the physics of multi-orbital Mott systems.

8 Mott Transition in Transition Metal Oxides

Mott transitions are a hallmark of strongly correlated electron systems and are experimentally found in transition metal oxides (TMOs). One of the most well-studied examples is vanadium sesquioxide, V_2O_3. The vanadium ion in V_2O_3 is in the $3+$ oxidation state, corresponding to an electronic configuration of $[\text{Ar}]3d^2$. Due to interatomic interactions, particularly along the crystallographic c-axis (perpendicular to the ab-plane), one of the two d electrons participates in covalent bonding with a neighbouring vanadium ion. This effectively reduces the system to a half-filled configuration with approximately one d electron per site — a situation where Mott physics becomes relevant.

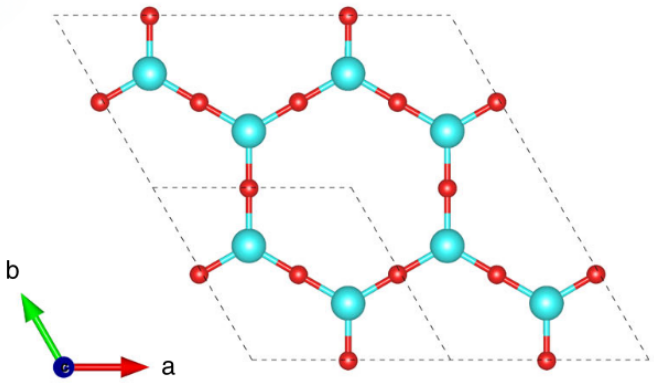

Figure 12: The crystal structure of V_2O_3 with sky-blue dots denoting V^{3+} and red dots denoting O^{2-}.

The treatment of such systems is difficult due to the presence of d-orbital degeneracy, which adds an additional orbital degrees of freedom to the already complex system. Experimentally, V_2O_3 exhibits a transition from an antiferromagnetic insulating (AFI) phase to a paramagnetic metallic (PM) phase at a Neel temperature of approximately $T_N \sim 160$ K. Interestingly, the metal-insulator transition coincides with the magnetic transition, and the overall transformation is first-order in nature, indicating a discontinuous change in the system's electronic structure.

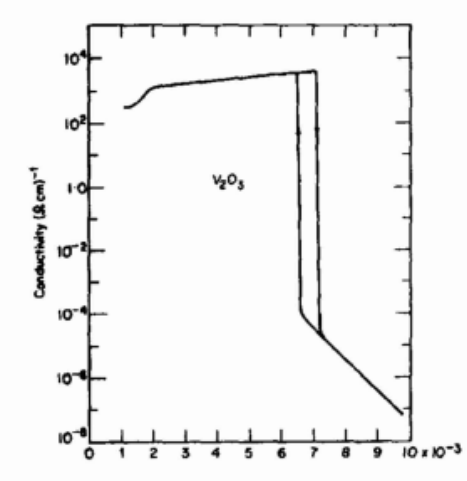

Figure 13: Temperature-dependent conductivity in V_2O_3, showing an abrupt fall in conductivity thus the Mott metal-insulator transition.

The Mott transition in V_2O_3 is fundamentally driven by the competition between the electron-electron interaction strength U and the electronic bandwidth W (or equivalently the hopping amplitude t). When the ratio U/t exceeds a critical threshold, the system favours localization due to strong Coulomb repulsion, resulting in an insulating state. Conversely, when U/t falls below the critical value, electrons delocalize and the system becomes metallic.

The ratio U/t can be experimentally tuned by external control parameters such as pressure and chemical doping. Applying hydrostatic pressure reduces the interatomic distance, thereby increasing the orbital overlap and increasing the hopping amplitude t. As a result, U/t decreases, leading to a suppression of the insulating phase and a reduction in the Neel temperature. On the other hand, chemical doping with larger ionic radius impurities (e.g., replacing V with Cr) causes lattice expansion, reduces overlap, decreases t, and effectively increases U/t, thereby favouring the insulating phase and enhancing magnetic order.

Chemical doping, in this context, acts as an analogue to negative pressure. The degree of doping can be mapped onto an effective pressure scale. The global phase diagram of V_2O_3, as a function of temperature and control parameters such as pressure or doping concentration, reveals three principal phases: a paramagnetic metal (PM), a paramagnetic insulator (PI), and an antiferromagnetic insulator (AFI). The insulator-to-metal transition between the PI and PM phases is first-order and is associated with a significant change in entropy due to the transition from a localized, entropy-poor state to a delocalized, entropy-rich state.

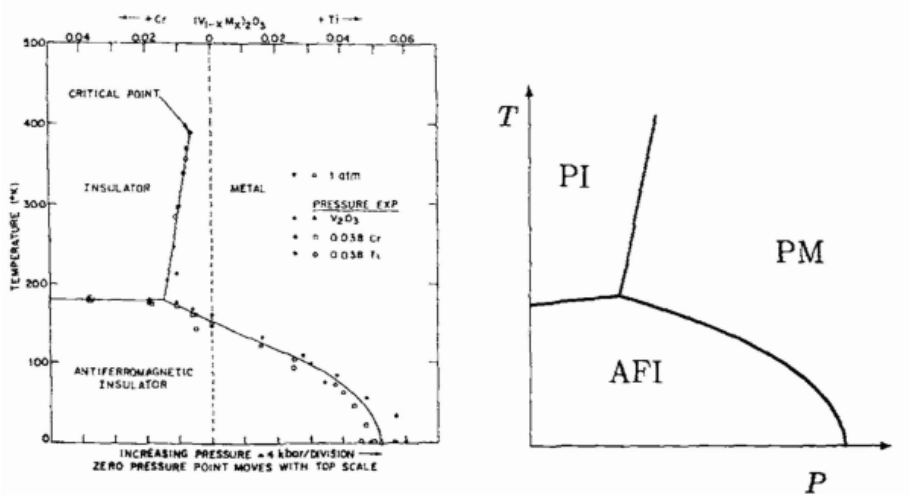

Figure 14: Generic phase diagram of V_2O_3 as a function of temperature and external tuning parameter (pressure or doping), showing the AFI, PI, and PM regions. In left figure, dashed vertical line shows zero effective pressure.

9 Super-exchange Mechanism

In many transition metal oxides such as V_2O_3, direct hopping between the d orbitals of neighbouring transition metal cations is strongly suppressed due to spatial separation and orbital symmetry. Instead, magnetic exchange interactions are mediated indirectly via the p orbitals of oxygen anions in between them — a mechanism known as *super-exchange*. This process is a higher-order virtual hopping phenomenon and plays a crucial role in establishing antiferromagnetic ordering in Mott insulating phases and separating Mott insulator from charge-transfer insulator.

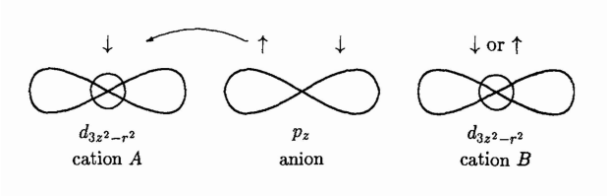

Figure 15: Diagram of super-exchange mechanism between two transition metal cations mediated via an intermediate oxygen anion.

To describe the super-exchange process microscopically, we consider a three-band model involving the transition metal d orbitals and the oxygen p orbitals. The Hamiltonian includes the on-site energies, hybridization between p and d states, and local Coulomb repulsion terms:

$$\begin{aligned} H =& \varepsilon_d \sum_{i,\sigma} d^\dagger_{i\sigma} d_{i\sigma} + \varepsilon_p \sum_{j,\sigma} p^\dagger_{j\sigma} p_{j\sigma} + \sum_{ij,\sigma\sigma_1} \Big((t_{pd})_{ij} d^\dagger_{i\sigma} p_{j\sigma_1} + \text{h.c.} \Big) \\ &+ U_{dd} \sum_i n_{di\uparrow} n_{di\downarrow} + U_{pp} \sum_j n_{pj\uparrow} n_{pj\downarrow} + U_{pd} \sum_{ij,\sigma\sigma_1} n_{di\sigma} n_{pj\sigma_1}. \end{aligned}$$

where $d^\dagger$ and $p^\dagger$ represent creation operators of electron, ε_d and ε_p denote the onsite energies of the transition metal d orbitals and oxygen p orbitals respectively, while t_{pd} represents the hopping amplitude between them. The interaction terms U_{dd}, U_{pp}, and U_{pd} correspond to Coulomb repulsion on the d sites, p sites, and between d-p sites, respectively. The above Hamiltonian is in electron representation where we quantify each energy term in terms of electron. Similarly one can think of a hole representation where $d^\dagger$ and $p^\dagger$ represent creation operators of holes, $\tilde{\varepsilon}$'s are on-site energies of holes and U's are described in similar fashion for holes.

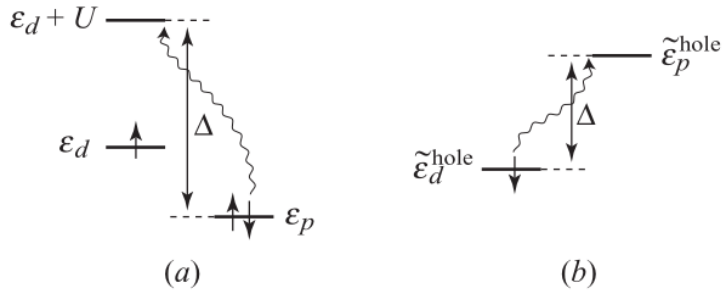

Figure 16: Virtual hopping processes contributing to super-exchange interaction: (a) in the electron representation and (b) in the hole representation.

The energy scale governing the virtual exchange process is the *charge transfer energy*, which in the electron picture is given by

$$\Delta = \varepsilon_d - \varepsilon_p + U_{dd},$$

and in the hole representation, corresponds to

$$\Delta = \tilde{\varepsilon}_p - \tilde{\varepsilon}_d,$$

where the tilde quantities denote effective orbital energies measured relative to the chemical potential in the hole basis. The resulting kinetic exchange processes are shown in fig. 16 for both electron and hole

representations. The interplay between U_{dd} and Δ dictates whether its charge-transfer insulator or Mott insulator.

The super-exchange interaction favours antiferromagnetic alignment of neighbouring spins due to the to the energy lowering associated with virtual hopping. This indirect exchange mechanism is central to understanding long-range magnetic ordering in Mott insulators and plays a key role in the low-energy physics of correlated transition metal oxides.

9.1 Charge Transfer Insulator vs Mott-Hubbard Insulator

In systems with strong p-d hybridization, two distinct super-exchange pathways emerge depending on the dominant energy scale—namely, the Hubbard repulsion U_{dd} or the charge-transfer energy $\Delta = \varepsilon_d - \varepsilon_p + U_{dd}$. These two pathways are shown in Fig. 17 in holes representation. Here all U's represents holes-holes interaction and t denotes holes hopping.

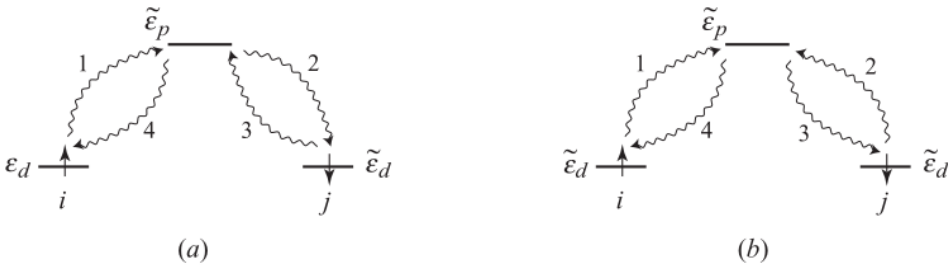

Figure 17: Two different super-exchange channels arising from (a) Mott-Hubbard type virtual hopping and (b) charge-transfer type virtual hopping.

Each super-exchange path contributes to an effective antiferromagnetic exchange coupling, described in the framework of the t-J model. For the Mott-Hubbard pathway (Fig. 17a), the intermediate energy states after each hopping are: Δ, U_{dd}, and Δ. Then the exchange coupling is given by

$$J_1 = \frac{2t_{pd}^4}{\Delta^2 U_{dd}} = \frac{2t_{dd}^2}{U_{dd}}, \quad \text{where } t_{dd} = \frac{t_{pd}^2}{\Delta}.$$

Its effectively a d-d hopping with hopping parameter t_{dd}. In contrast, for the charge-transfer pathway (Fig. 17b), the intermediate energy states after each hopping are: Δ, $2\Delta + U_{pp}$, and Δ. The exchange coupling takes the form

$$J_2 = \frac{4t_{pd}^4}{\Delta^2(2\Delta + U_{pp})}.$$

The total effective antiferromagnetic exchange coupling is the sum of the two contributions:

$$J_{\text{tot}} = J_1 + J_2 = t_{dd}^2 \left(\frac{1}{U_{dd}} + \frac{1}{\Delta + U_{pp}/2} \right).$$

The difference between two pathways are clear:

The relative magnitudes of Δ and U_{dd} determine the nature of the insulating phase. When $\Delta \gg U_{dd}$, the dominant exchange arises from the Mott-Hubbard mechanism. In this limit, the oxygen p orbital acts as a mere mediator, effectively reducing the problem to a one-band Hubbard model with d-d hopping. The lowest energy charge excitation in this case involves a d-d charge fluctuation:

$$\mathrm{p}^6\,\mathrm{d}_{(\mathrm{l})}{}^n\,\mathrm{d}_{(\mathrm{u})}{}^n \longrightarrow \mathrm{p}^6\,\mathrm{d}_{(\mathrm{l})}{}^{n-1}\,\mathrm{d}_{(\mathrm{u})}{}^{n+1},$$

indicating that the system is a *Mott-Hubbard insulator*. The $\mathrm{d_{(l)}}$ and $\mathrm{d_{(u)}}$ denote lower and upper sub-band of d-orbitals respectively.

On the other hand, in the regime $\Delta \ll U_{dd}$, the lowest energy excitation involves a transfer of an electron from a p orbital to a neighbouring d orbital:

$$\mathrm{d_{(l)}}^n\,\mathrm{p}^6\,\mathrm{d_{(u)}}^n \longrightarrow \mathrm{d_{(l)}}^n\,\mathrm{p}^5\,\mathrm{d_{(u)}}^{n+1},$$

a trait of a *charge transfer insulator*. In such materials, the gap is governed not by on-site Coulomb repulsion, but by the charge-transfer energy Δ from the oxide to the metal.

9.2 Zaanen-Sawatzky-Allen Phase Diagram

The distinction between Mott-Hubbard and charge-transfer insulators is formalized in the Zaanen-Sawatzky-Allen (ZSA) phase diagram, shown in Fig. 18. This phase diagram shows the electronic ground states of transition metal oxides as a function of U_{dd} and Δ. In the limit $U_{dd} < \Delta$, the system behaves as a Mott-Hubbard insulator, while for $\Delta < U_{dd}$, the charge-transfer nature dominates. The boundary between these regimes is material-specific, and some exhibit intermediate behaviour. In the zero limit of U_{dd}/t_{pd}, as expected, it behaves like metal. On the contrary, the metal-to-insulator boundary is very sharp.

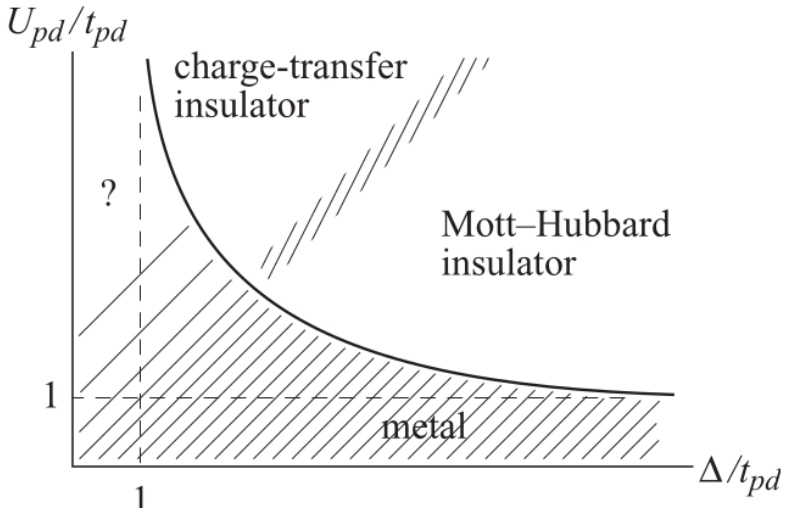

Figure 18: ZSA phase diagram showing different correlated insulating phases depending on the relative values of U_{dd} and Δ. **Note:** Correction in labeling: $U_{pd} \to U_{dd}$.

10 Dynamical Mean Field Theory

Dynamical Mean Field Theory (DMFT) is a non-perturbative method that enables the exact treatment of local quantum fluctuations in strongly correlated electron systems. A central quantity in finite-temperature quantum many-body theory is the thermal expectation value of an observable O, defined as

$$\langle O \rangle = \frac{1}{Z}\,\mathrm{Tr}\left(e^{-\beta(H-\mu N)}O\right), \tag{21}$$

where $Z = \mathrm{Tr}\left(e^{-\beta(H-\mu N)}\right)$ is the partition function, $\beta = 1/k_B T$ is the inverse temperature, μ is the chemical potential, and N is the particle number operator.

To describe the dynamics of the system, the single-particle (imaginary time) retarded Green's function (also referred to as the propagator) for a fermionic system is introduced as

$$G^R_{ij,\sigma}(\tau) = -i\theta(\tau)\left\langle\{c_{i\sigma}(\tau), c^\dagger_{j\sigma}\}\right\rangle, \tag{22}$$

where $c_i(\tau) = e^{H\tau}c_i e^{-H\tau}$ is the Heisenberg representation of the annihilation operator. In momentum space, the retarded Green's function takes the form

$$G^R_{k\sigma}(\tau) = -i\theta(\tau)\left\langle\{c_{k\sigma}(\tau), c^\dagger_{k\sigma}\}\right\rangle. \tag{23}$$

As an example, consider the non-interacting electron Hamiltonian

$$H_0 = \sum_{k\sigma} E(k)\, c^\dagger_{k\sigma} c_{k\sigma}, \tag{24}$$

whose corresponding retarded Green's function is given by

$$G_{k\sigma}(\tau) = -i\theta(\tau)\, e^{-iE(k)\tau}. \tag{25}$$

The spectral function $A_i(\omega)$, which encodes physical information such as the density of states, is related to the retarded Green's function via

$$A_i(\omega) = -2\ \mathrm{Im}\, G^R_{ii}(\omega), \tag{26}$$

where $G^R_{ii}(\omega)$ is Green's function in Frequency domain, arrived from doing Fourier transform of $G^R_{ii}(\tau)$. The retarded Green's function can be recovered from the spectral function using the relation

$$G^R_{ii}(\omega) = \int \frac{d\omega'}{\pi} \frac{A_i(\omega')}{\omega - \omega' + i\eta}. \tag{27}$$

For the above non-interacting electron case, the spectral function reduces to a delta function:

$$A_i(\omega) = 2\pi\, \delta(\omega - E(k)). \tag{28}$$

In general, the spectral function does not consist of delta peaks. In interacting systems, the spectral weight broadens due to finite lifetimes of excitations. This broadening can be captured by considering a time-decaying Green's function of the form

$$G^R_{ii}(\tau) = -i\theta(\tau)\, e^{-iE(k)\tau} e^{-\tau/\Gamma}, \tag{29}$$

which leads to a Lorentzian spectral function:

$$A_i(\omega) = -2\ \mathrm{Im}\, G^R_{ii}(\omega) = \frac{2/\Gamma}{(\omega - E(k))^2 + (1/\Gamma)^2}. \tag{30}$$

In the later discussion on the Hubbard model, we will encounter such spectral broadening arising from strong correlation effects.

11 Green's Function Calculation for Hubbard model in DMFT

The grand-canonical Hubbard Hamiltonian (considering chemical potential term) is given by

$$H_{\text{Hubbard}} = U \sum_j n_{j\uparrow} n_{j\downarrow} + \sum_{\langle ij \rangle \sigma} \left(t_{ij} c_{i\sigma}^\dagger c_{j\sigma} + \text{h.c.} \right) - \mu \sum_j (n_{j\uparrow} + n_{j\downarrow}) \tag{31}$$

In atomic limit the grand-canonical Hubbard Hamiltonian is given by

$$H_{\text{at}} = U \sum_j n_{j\uparrow} n_{j\downarrow} - \mu \sum_j (n_{j\uparrow} + n_{j\downarrow}). \tag{32}$$

Calculation of Green's function gives

$$G_{ii,\sigma}^R(\tau) = -i\theta(\tau) \left(e^{-(U-\mu)\tau} \langle n_{i,-\sigma} \rangle + e^{\mu\tau} \langle 1 - n_{i,-\sigma} \rangle \right), \tag{33}$$

and doing Fourier transform we get

$$G_{ii,\sigma}^R(\omega) = \frac{\langle n_{i,-\sigma} \rangle}{\omega - (U-\mu) + i\eta} + \frac{\langle 1 - n_{i,-\sigma} \rangle}{\omega + \mu + i\eta}. \tag{34}$$

According to the definition given in eq. (26), we arrive at the local spectral function

$$A_{i,\sigma}(\omega) = \langle n_{i,-\sigma} \rangle \, \delta(\omega - (U-\mu)) + \langle 1 - n_{i,-\sigma} \rangle \, \delta(\omega - \mu) \tag{35}$$

This atomic limit gives the two sharp Hubbard sub-bands at an energy difference of U. We expect the introduction of hopping term will broaden the bands.

The next concern is the band limit of Hubbard Hamiltonian (d-dim. cubic lattice) i.e.,

$$H_{\text{band}} = \sum_{k\sigma} (\varepsilon_k - \mu) c_{k\sigma}^\dagger c_{k\sigma}, \quad \varepsilon_k = -2t \sum_{i=1}^{d} \cos(k_i a). \tag{36}$$

The Green's function is given as

$$G_{k\sigma}^R(\omega) = \frac{1}{\omega - (\varepsilon_k - \mu)} \tag{37}$$

For our calculation we introduce a term called *self-energy*. In general, for an interacting fermionic system, the Green's function consists of the self-energy $\Sigma_\sigma(\omega)$, which encapsulates the effects of many-body interactions, and the retarded Green's function is of the form:

$$G_{k\sigma}^R(\omega) = \frac{1}{\omega - \varepsilon_k + \mu - \Sigma_\sigma(\omega)}. \tag{38}$$

It should be noted that the self-energy is assumed to be local (momentum-independent)

Return to the atomic limit case. One can write the Green's function as

$$\begin{aligned} G_{ii,\sigma}^R(\omega) &= \frac{n_{-\sigma}}{\omega - (U-\mu)} + \frac{1 - n_{-\sigma}}{\omega + \mu} \\ &= \frac{1}{\omega + \mu + \Sigma_\sigma^{\text{at}}(\omega)} \end{aligned} \tag{39}$$

where atomic self-energy is given by

$$\Sigma_\sigma^{\text{at}}(\omega) = Un_{-\sigma} + U^2 \frac{n_{-\sigma}(1-n_{-\sigma})}{\omega + \mu - U(1-n_{-\sigma})}. \tag{40}$$

The *Hubbard-I approximation* says the self-energy in (38) is same as the atomic self-energy i.e.,

$$\Sigma_\sigma(\omega) = \Sigma_\sigma^{\text{at}}(\omega).$$

The modified Green's function thus given by

$$G_{k\sigma}^R(\omega) = \frac{1}{\omega - \varepsilon_k + \mu - \Sigma_\sigma^{\text{at}}(\omega)} \tag{41}$$

$$= \frac{Z_\sigma^+(k)}{\omega + \mu + \omega_\sigma^+(k)} + \frac{Z_\sigma^-(k)}{\omega + \mu + \omega_\sigma^-(k)} \tag{42}$$

where the energy dispersion relation is

$$\omega_\sigma^\pm(k) = \frac{U + \varepsilon_k}{2} \pm \frac{1}{2}\sqrt{(U-\varepsilon_k)^2 + 4U\varepsilon_k n_{-\sigma}} \tag{43}$$

same as we got in eq. (7), and the spectral weight factors are

$$Z_\sigma^\pm(k) = \pm \frac{\omega_\sigma^\pm(k) - U(1-n_{-\sigma})}{\omega_\sigma^+(k) - \omega_\sigma^-(k)} \tag{44}$$

At exact half-filling $n_\uparrow = n_\downarrow = 1/2$ (mostly discussed in Mott transition case.) the energy dispersion gives two lowest Hubbard sub-bands

$$\omega_\sigma^\pm(k) = \frac{1}{2}\left(U + \varepsilon_k \pm \sqrt{U^2 + \varepsilon_k^2}\right). \tag{45}$$

and the gap for one electron excitation (the energy difference between lowest of upper and highest of lower sub-band) is calculated as

$$\Delta\mu = \sqrt{(W/2)^2 + U^2} - W/2 \tag{46}$$

where W is band gap (for d-dim. cubic lattice $W = 4td$). The Mott metal-insulator transition occurs when two bands start to overlap i.e., $\Delta\mu \approx 0$.

12 Spectral Weight Transfer

For the Hubbard model at half-filling, the Green's function $G_{k\sigma}^R(\omega)$ is expressed as the sum of contributions from the two Hubbard sub-bands:

$$G_{k\sigma}^R(\omega) = \frac{Z_\sigma^+(k)}{\omega + \mu + \omega_\sigma^+(k)} + \frac{Z_\sigma^-(k)}{\omega + \mu + \omega_\sigma^-(k)}$$

where energy dispersion relations $\omega_-(k)$ and $\omega_\sigma^+(k)$ correspond to the lower and upper Hubbard bands, respectively. The spectral weight factors $Z_\sigma^\pm(k)$ which reflects the distribution of states at a given energy, varies with the ratio U/t, where U is the on-site interaction strength and t is the hopping amplitude. A more accurate model using *Hubbard-III approximation*can give more realistic energy dispersion relations and spectral weights.

We found that as U/t increases, there is a noticeable transfer of spectral weight from the central quasiparticle peak to the "wings" of the spectrum. This behavior is illustrated in Figure 1, where the spectral function exhibits a three-peak structure. The central peak, corresponding to the quasiparticle excitation at the Fermi level, diminishes in weight as U/t is increased. At a critical value of U/t, the quasiparticle peak vanishes abruptly, and the density of states at the Fermi energy $\rho(\epsilon_F)$ drops discontinuously to zero, signaling the onset of a Mott transition.

This transition is first-order in nature, characterized by a sharp change in the spectral weight distribution. With further increases in U/t, the peaks become increasingly sharp, and ultimately, in the atomic limit ($U/t \to \infty$), the spectral function approaches δ-function-like peaks, indicating a complete localization of charge excitations.

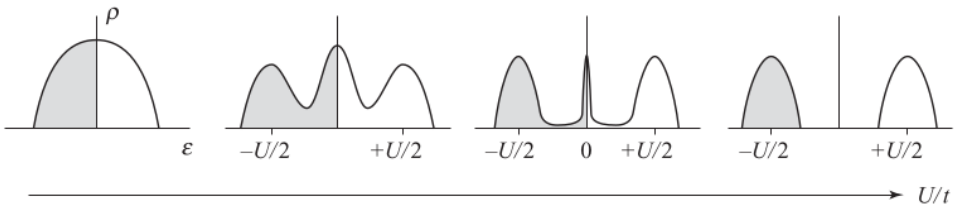

Figure 19: Spectral weight transfer in the Hubbard model. The figure shows the spectral function at various values of U/t, illustrating the transfer of weight from the central quasiparticle peak to the wings as U/t increases.

13 Conclusion

The Hubbard model, despite its simplicity, captures the essential physics of strongly correlated systems. The transition from delocalized to localized behaviour, driven by electron-electron interactions, leads to rich phenomena such as the opening of Hubbard sub-bands, spectral weight redistribution, and orbital ordering. In the strong-coupling limit, effective low-energy models like the t-J model reveal magnetic exchange processes fundamental to transition metal oxides. The inclusion of charge-transfer effects and orbital degeneracy places real materials in a broader context beyond the single-band Hubbard model. Finally, DMFT offers an excellent approach to access the full dynamics of the Mott transition, highlighting the coexistence of quasiparticles. Together these build a understanding of Mott physics across different regimes.

References

[1] P. Fazekas, *Lecture Notes on Electron Correlation and Magnetism* (World Scientific, Singapore, 1999).

[2] F. Gebhard, *The Mott Metal-Insulator Transition: Models and Methods* (Springer, Berlin, 1997).

[3] D. Khomskii, *Basic Aspects of the Quantum Theory of Solids: Order and Elementary Excitations* (Cambridge University Press, Cambridge, 2010).

[4] H. Bruus and K. Flensberg, *Many-Body Quantum Theory in Condensed Matter Physics: An Introduction* (Oxford University Press, Oxford, 2004).

[5] D. Vollhardt, K. Byczuk, and M. Kollar, *Dynamical Mean-Field Theory*, arXiv:1109.4833 [cond-mat.str-el] (2011).